On the benefit of direct wheel torque control for longitudinal comfort enhancement on uneven roads

On the benefit of direct wheel torque control for longitudinal comfort enhancement on uneven roads

Davide Lazzarini
Department of Mechanical and Aerospace Engineering
Politecnico di Torino
Turin, 10129, Italy
https://orcid.org/0009-0001-8703-5040

Antonio Tota
Department of Mechanical and Aerospace Engineering
Politecnico di Torino
Turin, 10129, Italy
https://orcid.org/0000-0002-7151-8873

Aldo Sorniotti
Department of Mechanical and Aerospace Engineering
Politecnico di Torino
Turin, 10129, Italy
https://orcid.org/0000-0002-4848-058X

***Abstract*—Ride comfort is highly affected by road irregularities which cause oscillations in the vertical and longitudinal accelerations. While most studies focus on attenuating the vertical oscillations, a few of them focus on the longitudinal component. Moreover, even fewer in this context compare the control performance of different powertrain architectures, mainly focusing on localized road events. The aim of this research is to demonstrate the effectiveness of in-wheel motor (IWM) architecture for improving vehicle comfort. This paper presents a nonlinear model predictive control (NMPC) strategy, enhanced with the road height profile as preview information. The proposed control architecture is implemented on a vehicle model with two different powertrain configurations: one with four IWMs and another with four conventional on-board motors (OBMs). Performance is assessed across three road profiles of increasing roughness. The results demonstrate that IWM control improves ride comfort significantly compared to the uncontrolled vehicle, achieving an acceleration oscillations reduction of 41% on A-class roads and 31% on C-class roads. On the contrary, the OBM configuration only achieves improvements of 20% and 12%, respectively.**

Keywords—Fully electric vehicle, comfort enhancement, nonlinear model predictive control

I. INTRODUCTION

Ride comfort is one of the main aspects of vehicle design, directly affecting passenger wellness. Road irregularities cause vertical and longitudinal acceleration oscillations of the sprung and unsprung masses, playing an important role in vehicle drivability [1]. While vertical oscillations have been widely studied, only few authors analyzed the longitudinal component, despite its relevance [3]. In fact, due to its higher frequency, it also plays an important role in ride comfort [5]. To effectively control these fast dynamics, a fast response time of the actuation system is required. To this aim, electric machines (EMs) demonstrated to be a better choice with respect to (w.r.t.) internal combustion engines. With the introduction of electric vehicles (EVs), different powertrain configurations, e.g., with OBMs, with and without mechanical linkages between the vehicle sides, and with IWMs, have been developed.

Few studies developed control logics to compensate the longitudinal acceleration oscillations caused by road irregularities. In [6], Vidal et al. present a NMPC logic to effectively control an EV equipped with four IWMs. In [7], Stano et al. compared the IWM configuration with two on-board configurations, one with four OBMs and one with two OBMs, one per axle, connected to the wheels through the open differentials. Mainly localized road events have been tested to compare the architectures.

The aim of this research is to compare the ride comfort improvement achieved with a NMPC logic, enhanced with road profile height preview, on different EV powertrain architectures, i.e., with four IWMs and with four OBMs, on different uneven roads with increasing roughness.

II. SIMULATION ENVIRONMENT

A. Vehicle configurations

A fully EV, with two different powertrain configurations is implemented in a MATLAB Simulink environment. The two analyzed powertrains are composed by four IWMs and four OBMs, where the latter ones are connected to the wheels through single-speed double-stage gearboxes and transmission shafts. Some of the main vehicle parameters are listed in Table I.

TABLE I. VEHICLE PARAMETERS

Description	Symbol	Value	Unit
Front semi-wheelbase	a	1.473	[m]
Rear semi-wheelbase	b	1.455	[m]
Centre of gravity height	h_g	0.631	[m]
Wheel radius	R_u	0.373	[m]
In-wheel configuration			
Sprung mass	m_b	2593	[kg]
Unsprung mass	m_u	65	[kg]
Mass moment of inertia of the wheel hub	$J_{u,y}$	1.6	[kgm^2]
EM time constant	τ_m	5.7	[ms]
Maximum EM torque	$T_{m,max}$	1500	[Nm]
On-board configuration			
Sprung mass	m_b	2789	[kg]
Unsprung mass	m_u	30	[kg]
Mass moment of inertia of the wheel hub	$J_{u,y}$	1.39	[kgm^2]
EM time constant	τ_m	5.7	[ms]
Maximum EM torque	$T_{m,max}$	350	[Nm]
Torsional stiffness of the transmission shaft	k_s	7700	[Nm/rad]
Torsional damping of the transmission shaft	c_s	47	[Nms/rad]
Gar ratio of the transmission gearbox	i_t	4.5	[-]
Efficiency of the transmission gearbox	η_t	0.96	[-]
Backlash of the transmission gearbox at the output shaft	2α	1.26	[deg]

The vehicle dynamics, whose model has been validated through experimental testing, is described by 15 degrees-of-freedom (DOFs). The motion of the sprung mass, i.e., the vehicle body, is simulated through 3 DOFs related to the longitudinal, vertical and pitch dynamics. Similarly, the motion of the unsprung mass, i.e., the wheel hub, is described by 3 DOFs related to the longitudinal, vertical and rotational dynamics. In addition, the traction forces and the rolling resistance moments are calculated through the MF-Swift tyre model [8]. Finally, the EM dynamics is represented by a first order transfer function and, only for the OBM configuration, the torsional dynamics of the

transmission shafts is characterized by torsional stiffness and damping meanwhile the gearbox is modeled with an equivalent angular backlash between their teeth and a constant efficiency, as these properties heavily affect the wheel torque transmission as described in [9].

B. Road profiles definition

For the purpose of this research, three different uneven road profiles, shown in Fig. 1, are simulated. Fig. 1a shows the displacement power spectral density (PSD) G_d of the road unevenness in frequency domain, which, according to the ISO-8608-2016 [10], classifies the roads as A, B and C-classes. Finally, Fig. 1b shows the road height z_r in space domain.

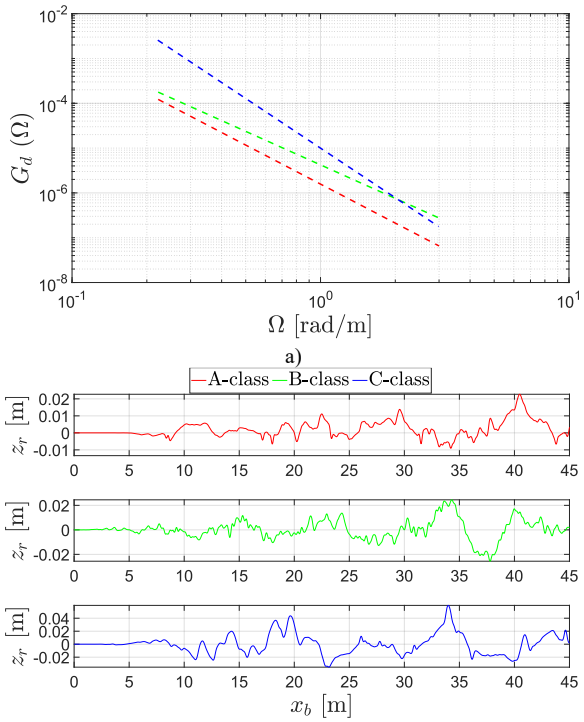

Fig. 1. Uneven road profiles: (a) power spectral density in frequency domain and (b) road height in space domain.

III. Control System

A. Overview of the control architecture

The control architecture of this study, highlighted in Fig. 2 by the gray block 'longitudinal controllers', consists of the following blocks.

1. The enveloping model, proposed by Schmeitz in [11] with road preview, which, based on the current wheel corner longitudinal position and speed, $x_{u,ij}$ and $\dot{x}_{u,ij}$, and the road profile height z_r, provides the effective road height w_{ij} and slope $\beta_{y,ij}$ along the prediction horizon t_h, with a constant sampling time t_s. The subscript 'i' identifies the front 'f' and rear 'r' axles, while the subscript 'j' defines the vehicle side, left 'l' and right 'r'.
2. The NMPC block, which, based on the main vehicle states $\hat{x}$, the requested torque at the motor level $T_{m,req,ij}$, w_{ij} and $\beta_{y,ij}$, provides the torque correction $\Delta T_{m,ij}$. The corrected torque $T_{m,cor,ij}$, which corresponds to the sum between $T_{m,req,ij}$ and $\Delta T_{m,ij}$, is then provided, as reference, to the EM.

The above-mentioned blocks are specific to a single corner. Hence, the whole control architecture is composed of 4 NMPCs, each one individually controlling a single corner, and 4 enveloping models with road preview. The remaining blocks are part of the simulation environment:

1. The driver model, which provides the accelerator pedal position APP.
2. The drivability map, which provides the requested total torque $T_{m,req}$, as a function of APP and the longitudinal speed of the sprung mass $\dot{x}_b$.
3. The front-to-total (F2T) torque distribution controller, which splits the request between the two axles. For this analysis, the F2T distribution ratio is set equal to 0.5, i.e., $T_{m,req,ij} = T_{m,req}/4$.
4. The plant model and MF-Swift tyre model, which describes the vehicle, wheels and tyre dynamics.
5. The road profile block, which provides the road height to the control architecture and tyre model.

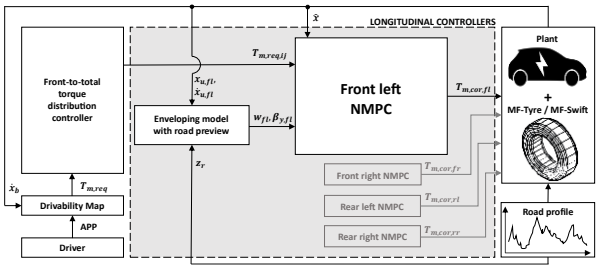

Fig. 2. Schematic of the control architecture and simulation environment.

B. NMPC formulation

The internal model of the NMPC, i.e., the prediction model, and the optimal control problem (OCP) are described below.

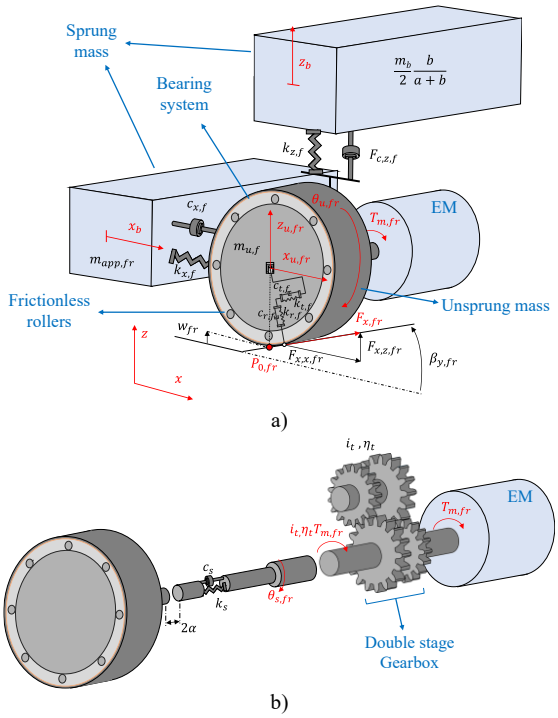

Fig. 3. Front-right NMPC internal model dynamics: (a) representation of the entire model of the IWM configuration and (b) representation of the single-speed double stage gearbox and transmission shaft dynamics, exclusive for the OBM configurations.

Since each NMPCs is employed for a single corner, the prediction model only consists of the dynamics of the corresponding corner. The following differential equations, as well as the OCP formulation, refer to the front-right corner:

- The vertical dynamics of the sprung mass:

$$\frac{m_b}{2}\frac{b}{a+b}\ddot{z}_{b,fr} = -F_{k,z,fr} - F_{c,z,fr} + \Delta F_{z,b} - F_{z,ap,fr} \quad (1)$$

where $z_{b,fr}$ is the vertical displacement of the sprung mass; m_b is the sprung mass; a and b are the front and rear semi-wheelbases; $F_{k,z,fr}$ and $F_{c,z,fr}$ are the vertical forces associated with the stiffness and damping characteristics, respectively, of the suspension system; $\Delta F_{z,b}$ is the longitudinal load transfer; and $F_{z,ap,fr}$ is the force generated by the suspension anti-properties.

- The vertical dynamics of the unsprung mass:

$$m_u\ddot{z}_{u,fr} = F_{k,z,fr} + F_{c,z,fr} + F_{r,z,fr} - F_{t,z,fr} + F_{x,z,fr} + F_{z,ap,fr} \quad (2)$$

where $z_{u,fr}$ is the vertical displacement of the unsprung mass; m_u is the unsprung mass; $F_{r,z,fr}$ and $F_{t,z,fr}$ are the vertical component of the radial and tangential forces of the tyre model, provided by the interaction with the road profile; and $F_{x,z,fr}$ is the vertical component of the traction force $F_{x,fr}$.

- The longitudinal dynamics of the sprung mass:

$$m_{app,fr}\ddot{x}_{b,fr} = -F_{k,x,fr} - F_{c,x,fr} + \frac{i_t\eta_t}{R_u}\left[T_{m,req,rl} + T_{m,req,rr} + T_{m,req,fl}\right] - F_{drag} - F_{roll,rl} - F_{roll,rr} - F_{roll,fl} \quad (3)$$

where $x_{b,fr}$ is the longitudinal displacement of the sprung mass; $m_{app,fr}$ is the apparent mass; $F_{k,x,fr}$ and $F_{c,x,fr}$ are the longitudinal component of the stiffness and damping forces of the suspension linkages; i_t and η_t are the transmission ratio and efficiency, which have unitary value in case of IWMs; R_u is the wheel radius; F_{drag} is the aerodynamic resistance force; and $F_{roll,ij}$ is the rolling resistance force of the ij-th corner.

- The longitudinal dynamics of the unsprung mass:

$$m_u\ddot{x}_{u,fr} = F_{k,x,fr} + F_{c,x,fr} - F_{r,x,fr} - F_{t,x,fr} + F_{x,x,fr} \quad (4)$$

where $x_{u,fr}$ is the longitudinal displacement of the unsprung mass; $F_{r,x,fr}$ and $F_{t,x,fr}$ are the longitudinal component of the radial and tangential forces of the tyre model; and $F_{x,x,fr}$ is the longitudinal component of the traction force.

- The rotational dynamics of the unsprung mass:

$$J_{u,y}\ddot{\theta}_{u,fr} = T_{w,fr} - F_{x,fr}R_u - M_{roll,fr} \quad (5)$$

where $\dot{\theta}_{u,fr}$ is the angular velocity of the wheel; $J_{u,y}$ is the wheel mass moment of inertia; $T_{w,fr}$ is the motor torque at the wheel level, which is equal to actual EM torque $T_{m,fr}$ in case of IWMs; and $M_{roll,fr}$ is the rolling resistance moment.

- The drivetrain torsional dynamics, included only in the OBM prediction model:

$$J_{s,eq}\ddot{\theta}_{s,fr} = i_t\eta_t T_{m,fr} - T_{w,fr} \quad (6)$$

where $\dot{\theta}_{s,fr}$ is the angular velocity of the transmission shaft; $J_{s,eq}$ is the equivalent inertia of the entire drivetrain, i.e, the transmission shaft and EM, at the wheel level.

- The EM dynamics:

$$\tau_m\dot{T}_{m,fr} = T_{m,cor,fr} - T_{m,fr} \quad (7)$$

where τ_m is the EM time constant.

For an graphical visualization of the considered dynamics, Fig. 3 shows the main vehicle parameters and DOFs included in the internal model: on the one hand, Fig. 3a exactly matches the internal model formulation for the IWM configuration; on the other hand, Fig. 3b shows the torsional dynamics included in the OBM configuration. A more detailed description of the involved forces of both configurations is included in [7].

The optimal control problem of the front-right NMPC is formulated as follows.

$$\begin{aligned}&\underset{U}{\operatorname{argmin}}\, J := J_t + J_s = \frac{1}{2}\left\|z_{fr,N_h} - z_{fr,ref,N_h}\right\|_{Q_t}^2 + \frac{1}{2}\sum_{k=0}^{N_h-1}\left[\left\|z_{fr,k} - z_{fr,ref,k}\right\|_Q^2 + \left\|u_{fr,k}\right\|_R^2\right]\\ &\text{s.t.}\\ &x_{fr,0} = x_{fr,in}\\ &x_{fr,k+1} = f_{pm}\left(x_{fr,k}, u_{fr,k}, p_{fr,k}\right)\\ &z_{fr,k} = g_{pm}\left(x_{fr,k}, u_{fr,k}, p_{fr,k}\right)\\ &T_{m,lb} \le T_{m,req,fr} + \Delta T_{m,fr} \le T_{m,ub}\end{aligned} \quad (8)$$

where J is the cost function, composed by its terminal and stage parts, J_t and J_s; $U_{fr} = \left[u_{fr,0}, u_{fr,1}, \dots, u_{fr,k}, \dots, u_{fr,N_h}\right]$ is the control action sequence; k is a generic step; N_h is the number of prediction steps; Q and Q_t are the stage and terminal cost function weight matrices associated with the output errors $z_{fr} - z_{fr,ref}$; R is the stage cost function weight matrix associated with the control action; f_{pm} and g_{pm} are the functions associated with the states and outputs of the NMPC internal model, respectively; $x_{fr,k}$, $u_{fr,k}$ and $p_{fr,k}$ are the state, control action and online parameter vectors at the k-th step; and $T_{m,lb}$ and $T_{m,ub}$ are the lower and upper bounds of the EM torque.

The output and its reference are defined as follower, respectively:

$$\begin{aligned}z_{fr} &= \ddot{x}_{b,fr}\\ z_{fr,ref} &= \ddot{x}_{b,ref}\end{aligned} \quad (9)$$

where the reference longitudinal acceleration of the sprung mass $\ddot{x}_{b,ref}$ is calculated as:

$$\ddot{x}_{b,ref} = \left[\sum_{i=f,r}\sum_{j=l,r}\frac{T_{w,req,ij}}{R_u} - F_{roll} - F_{drag}\right]\frac{1}{m_b + 4m_u + \frac{4J_{u,y}}{R_u^2}} \quad (10)$$

where $T_{w,req,ij}$ is the requested torque at the wheel level ($T_{w,req,ij} = T_{m,req,ij}$ for the IWM configuration and $T_{w,req,ij} = i_t\eta_t T_{m,req,ij}$ for the OBM configuration); R_u is the wheel radius; F_{roll} is the rolling resistance force; and F_{drag} is the aerodynamic resistance force.

The remaining vectors are as follows:

$$\begin{aligned}x_{fr} &= [\dot{z}_{b,fr}, z_{b,fr}, \dot{z}_{u,fr}, z_{u,fr},\\ &\quad \dot{x}_{b,fr}, x_{b,fr}, \dot{x}_{u,fr}, x_{u,fr},\\ &\quad \dot{\theta}_{u,fr}, T_{m,fr}, \theta_{u,fr}, \dot{\theta}_{s,fr}, \theta_{s,fr}]\\ u_{fr} &= \Delta T_{m,fr}\\ p_{fr} &= [w_{fr}, \beta_{y,fr},\\ &\quad T_{m,req,fl}, T_{m,req,fr}, T_{m,req,rl}, T_{m,req,rr}]\end{aligned} \quad (11)$$

where $\theta_{u,fr}$, $\dot{\theta}_{s,fr}$ and $\theta_{s,fr}$ are only included in the state vector of the OBM configuration.

C. *Road preview information*

The online parameter vector p is composed by constant values along the prediction steps, unless for w and β_y, which are obtained by the preview information. In fact, in the proposed control logic, the preview allows to know in advance the road profile height, as shown in Fig. 4.

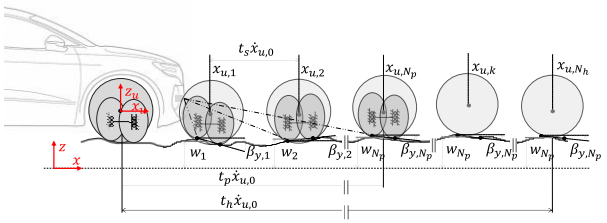

Fig. 4. Road preview schematic.

The preview is obtained under the assumption of having constant speed $\dot{x}_{u,0}$ along the preview horizon t_p. So, by obtaining the future wheel positions $x_{u,k}$, the corresponding w_k and $\beta_{y,k}$ can be calculated with the enveloping model. t_p is typically set shorter than t_h due to the increasing inaccuracy of predictions over longer time steps. For this reason, w_{N_p} and β_{y,N_p}, i.e., the values obtained through the preview at the last preview step N_p, are kept constant for the remaining prediction steps from t_p to t_h.

IV. Results

In this section, 5 vehicle configurations are analyzed. Passive$_{\text{IWM}}$ and Passive$_{\text{OMB}}$ correspond to the vehicle without control logic, i.e., with the provided torque exactly equal to the request, apart from the delay brought by the motor torque dynamics. The subscripts 'IWM' and 'OBM' indicate the powertrain configuration. NMPC$_{\text{base,IWM}}$ corresponds to the controlled vehicle model, without preview implementation, i.e., with constant w and β over t_h. Finally, NMPC$_{\text{prev,IWM}}$ and NMPC$_{\text{prev,OBM}}$ are the controlled versions with preview information on the road profile.

The NMPC parameters, t_h and t_p, are set equal to 30 and 25 ms, respectively, as a sensitivity analysis in [7] has identified them as optimal. In addition, t_s is set equal to 1 ms.

To evaluate the performance, two key performance indicators (KPIs) are considered.

1. $\Delta\ddot{x}_{b,\text{RMS}}$, i.e., the root mean square value of the longitudinal acceleration error $\ddot{x}_b - \ddot{x}_{b,ref}$:

$$\Delta\ddot{x}_{b,\text{RMS}} = \sqrt{\frac{1}{T_2-T_1}\int_{T_1}^{T_2}\left[\ddot{x}_b - \ddot{x}_{b,ref}\right]^2 dt} \tag{12}$$

where T_1 and T_2 are the start and end time instants of the relevant part of the simulation.

2. $\Delta\ddot{x}_{b,\text{VDV}}$, i.e., the fourth power vibration dose value of the longitudinal acceleration error $\ddot{x}_b - \ddot{x}_{b,ref}$:

$$\Delta\ddot{x}_{b,\text{VDV}} = \sqrt[4]{\int_{T_1}^{T_2}\left[\ddot{x}_b - \ddot{x}_{b,ref}\right]^4 dt} \tag{13}$$

To analyze the full potential of the controlled configurations, i.e., to achieve the best KPIs, all NMPC architectures have been tuned for each individual road scenario.

Fig. 5 compares the controlled architectures, with and without preview information, against the passive vehicle, for the IWM configuration, on the A-class road. The vehicle passes through the uneven road with an initial speed of 40 km/h and a constant zero torque demand. NMPC$_{\text{prev,IWM}}$ is able to provide more effective torque correction in advance, e.g., at 22 m, to better attenuate the acceleration. NMPC$_{\text{base,IWM}}$ and NMPC$_{\text{prev,IWM}}$ improve $\Delta\ddot{x}_{b,\text{RMS}}$ by 31% and 41% and $\Delta\ddot{x}_{b,\text{VDV}}$ by 25% and 40% w.r.t. the passive vehicle, respectively. The absolute values of the KPIs are included in Table II, which also contains the KPIs of the following analysis.

Fig. 5. Benefit of preview information on the A-class road.

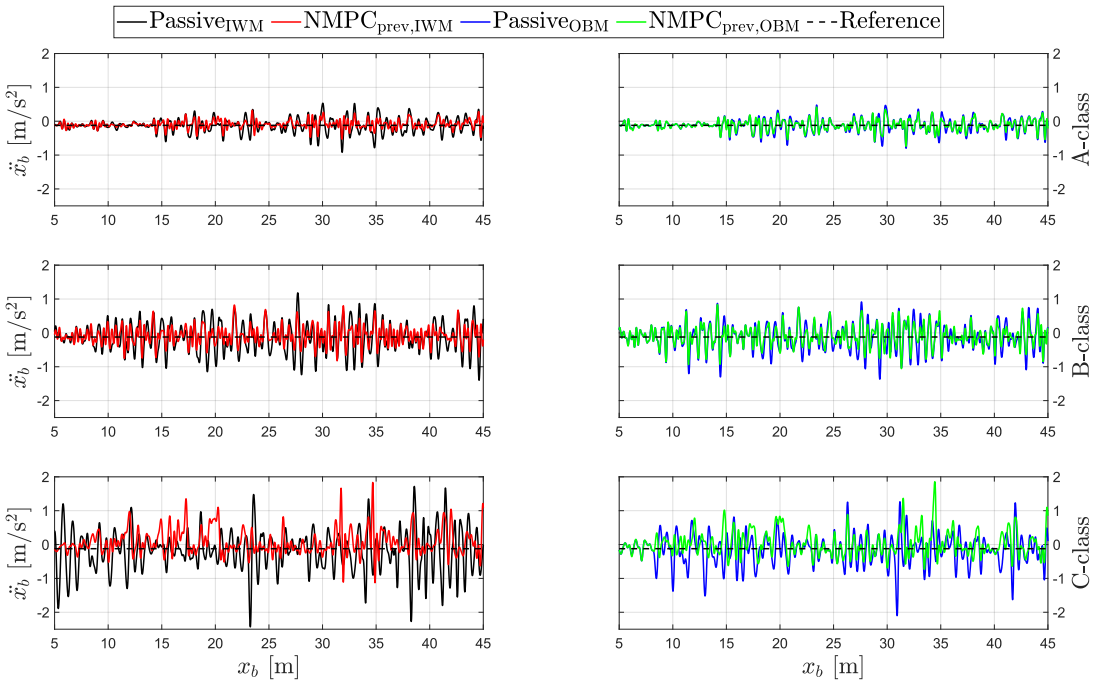

Fig. 6. Comparison between IWM and OBM control on the A, B and C-class roads.

Fig. 6 shows how the road profile unevenness differently affects the two architectures, IWM and OBM, and how the control logics are able to compensate those oscillations. Going from A-class to C-class, all KPIs get worse, with a significant impact on the passive vehicle with IWM powertrain, due to the large increase in the unsprung mass w.r.t. the OBM architecture: the absolute value of the difference in terms of $\Delta\ddot{x}_{b,\mathrm{RMS}}$ between Passive$_{IWM}$ and Passive$_{OBM}$ increases from 0.017 to 0.164 m/s^2. However, the IWM control appears promising, showing only a slight degradation of the percentage improvement of $\Delta\ddot{x}_{b,\mathrm{RMS}}$ w.r.t. the passive vehicle, going from 41% for the A-class road to 37% for the B-class and 31% for the C-class. On the contrary, the OBM control is not able to achieve similar performance, reaching a percentage improvement w.r.t. the passive configuration of 18%, 20% and 12% for the A, B and C-class roads, respectively. Similar trend is associated with $\Delta\ddot{x}_{b,\mathrm{VDV}}$, whose improvement w.r.t. the passive vehicle reaches values of 27% and 6% on the C-class road for NMPC$_{prev,IWM}$ and NMPC$_{prev,OBM}$, respectively.

TABLE II. KEY PERFORMANCE INDICATORS

Configuration	$\Delta\ddot{x}_{b,\mathrm{RMS}}$ [m/s^2]	$\Delta\ddot{x}_{b,\mathrm{VDV}}$ [m/s$^{1.75}$]
A-class		
Passive$_{IWM}$	0.203	0.397
NMPC$_{base,IWM}$	0.141	0.297
NMPC$_{prev,IWM}$	0.120	0.237
Passive$_{OBM}$	0.186	0.360
NMPC$_{prev,OBM}$	0.152	0.296
B-class		
Passive$_{IWM}$	0.422	0.759
NMPC$_{prev,IWM}$	0.266	0.512
Passive$_{OBM}$	0.374	0.688
NMPC$_{prev,OBM}$	0.298	0.556
C-class		
Passive$_{IWM}$	0.598	1.177
NMPC$_{prev,IWM}$	0.410	0.863
Passive$_{OBM}$	0.434	0.877
NMPC$_{prev,OBM}$	0.383	0.822

Since for the majority of time vehicles operate on Class-C roads, this is the area with the highest impact. It is important also to note that the actual acceleration values as the actual ride comfort values on rougher road are lower on OBM configurations. However, even if vehicles with IWM powertrain configurations achieve worse ride comfort, this architecture is beneficial for many other controller integrations, such as traction control, stability control and direct yaw moment control.

V. CONCLUSIONS

Vehicles equipped with IWMs, compared to OBM architectures, tend to be more affected by road irregularities, due to the unsprung mass increase. However, IWM control can compensate this aspect achieving better KPIs than the OBM configuration. The main outcomes are listed below.

- The passive vehicle, i.e., without control logic, with IWM architecture, Passive$_{IWM}$, achieves a 9% comfort degradation, in terms of $\Delta\ddot{x}_{b,\mathrm{RMS}}$, w.r.t. the OBM configuration, Passive$_{OBM}$, on A-class road. However, the NMPC logic with road preview improves comfort, achieving an improvement of 41% w.r.t. the passive vehicle, which corresponds to an improvement of 21% w.r.t. the controlled OBM configuration.
- The controlled vehicle with OBM architecture and with road preview, NMPC$_{prev,OBM}$, has worse KPIs than the NMPC without preview of the IWM configuration. This proves that the responsiveness of the powertrain architecture is so relevant that even the preview implementation cannot reach its full potential.
- From A-class to C-class roads, the improvement brought by the control logic w.r.t. the passive vehicle becomes less significant for the OBM configuration, reaching the lowest $\Delta\ddot{x}_{b,\mathrm{RMS}}$ and $\Delta\ddot{x}_{b,\mathrm{VDV}}$, equal to 12% and 6%, respectively. The IWM control instead

demonstrates its robustness, achieving at least 31% and 27% improvements for $\Delta\ddot{x}_{b,\mathrm{RMS}}$ and $\Delta\ddot{x}_{b,\mathrm{VDV}}$, respectively.

Future work will focus on the evaluation of IWM and OBM control on roads with varying friction conditions, with integrated ride comfort and traction control functionalities.

ACKNOWLEDGMENTS

This research was supported by the European Union's Horizon Europe research and innovation program under grant 101138110.

REFERENCES

[1] Burdzik, R. (2014). Identification of structure and directional distribution of vibration transferred to car-body from road roughness. Journal of Vibroengineering, 16(1), 324-333.

[2] Žuraulis, V., Levulytė, L., and Sokolovskij, E. (2014). The impact of road roughness on the duration of contact between a vehicle wheel and road surface. Transport, 29(4), 431-439. DOI: 10.3846/16484142.2014.984330.

[3] Yamada, S., Beauduin, T., Fujimoto, H., Kanou T., and Katsuyama, E. (2017). Model-based longitudinal vibration suppression control for electric vehicles with geared in-wheel motors. 2017 IEEE International Conference on Advanced Intelligent Mechatronics (AIM), Munich, Germany, 517-522. DOI: 10.1109/AIM.2017.8014069.

[4] Yamada, S., Beauduin, T., Fujimoto, H., Kanou T., and Katsuyama, E. (2022). Active Model-Based Suppression of Secondary Ride for Electric Vehicles With In-Wheel Motors. IEEE/ASME Transactions on Mechatronics, 27(6), 5637-5646. DOI: 10.1109/TMECH.2022.3187414.

[5] Hamadi, N., Ameddah, D., and Imine, H. (2014). Investigation of the Adherence Influence on the Dynamic Behavior of the Vehicle. International Journal of Hybrid Information Technology, 7(5), 85-102. DOI: 10.14257/ijhit.2014.7.5.08.

[6] Vidal, V., Stano, P., Tavolo, G., Dhanes, M., Tavernini, D., Gruber, P., and Sorniotti, A. (2022). On Pre-Emptive In-Wheel Motor Control for Reducing the Longitudinal Acceleration Oscillations Caused by Road Irregularities. IEEE Transactions on Vehicular Technology, 71(9), 9322-9337, DOI: 10.1109/TVT.2022.3172172.

[7] Stano, P., Lazzarini, D., Santoro, S., Mihalkov, M., Montanaro, U., Vigliani, A., Ferrara, Dhaens, M., and Sorniotti, A. (2024). On-board electric powertrain control for the compensation of the longitudinal acceleration oscillations caused by road irregularities. Mechanism and Machine Theory, 202, 105759. DOI: 10.1016/j.mechmachtheory.2024.105759.

[8] Siemens Digital Industries Software, (2020). Simcenter Tire – MF-Tyre/MF-Swift User Manual.

[9] Guercioni, G.R., Galvagno, E., Tota, A., Vigliani, A., and Zhao, T. (2018). Driveline backlash and half-shaft torque estimation for electric powertrains control. SAE Technical Paper, 2018-01-1345. DOI: 10.4271/2018-01-1345.

[10] ISO 8608:2016, Mechanical vibration, Road surface profiles.

[11] Schmeitz, A.J.C., Jansen, S., Pacejka, H.B., Davis, J.C., Kota, N.N., Liang, C.G., and Lodewijks, G. (2004). Application of a semi-empirical dynamic tyre model for rolling over arbitrary road profiles. International Journal of Vehicle Design, 36(2-3), 194-215. DOI: 10.1504/IJVD.2004.005356.